Comparison of Iodine-125-BMIPP and Thallium-201 in Myocardial Hypoperfusion

Christopher P. Reinhardt, Howard Weinstein, Robin Marcel and Jeffrey A. Leppo

Myocardial Isotope Research Lab, Departments of Nuclear Medicine and Medicine (Cardiovascular Division), University of Massachusetts Medical Center, Worcester, Massachusetts

Radiolabeled fatty acids such as 15-(*p*-iodophenyl)-3-R,S-methylpentadecanoic acid (BMIPP) have unique metabolic properties of potential use as myocardial perfusion tracers. Accordingly, we compared the in vivo pattern of uptake of BMIPP and ^{201}Tl in hypoperfused rabbit myocardium. **Methods:** Animals were intubated, ventilated and their arterial pressures monitored. A left thoracotomy was performed. After ligation of a major branch of the circumflex artery, an intravenous injection of BMIPP or BMIPP/^{201}Tl was given. Radiolabeled microspheres were used to document the area of risk. After the circulation period, the animals were killed. Tracer deposition within the hearts was determined by either dual-tracer autoradiography (Protocol I) or by segmental tissue analysis (Protocol II). **Results:** Dual-tracer autoradiographic activity profiles for BMIPP were comparable to those of ^{201}Tl. Moreover, the two tracers yielded similar values for normal-to-defect contrast and defect size. The myocardial activity concentration of BMIPP for both protocols correlated strongly with coronary blood flow and compared favorably with ^{201}Tl. **Conclusion:** BMIPP and ^{201}Tl accurately delineate areas of hypoperfusion distal to a coronary occlusion. Therefore, differences in the myocardial distribution of BMIPP and ^{201}Tl in clinical studies may be related to cellular fatty acid metabolism.

Key Words: iodine-125-BMIPP; thallium-201; myocardial hypoperfusion; dual-tracer autoradiography; segmental tissue analysis

J Nucl Med 1995; 36:1645–1653

Under normal aerobic conditions, the energy required by the myocardium is met primarily by the oxidation of free fatty acids (*1,2*). As a result, radiolabeled free fatty acids have been developed to assess myocardial fatty acid metabolism. Positron radiolabeled free fatty acids, such as ^{11}C-palmitic acid (*3–5*), can be used to evaluate regional fatty acid metabolism. The expense of maintaining an on-site cyclotron to produce short-lived, positron-emitting radiopharmaceuticals, however, has focused attention on the development of gamma-emitting, iodinated free fatty acids.

One iodinated free fatty acid, 15-(*p*-iodophenyl)-3-R,S-methylpentadecanoic acid (BMIPP), has shown unique metabolic properties for potential use in assessing myocardial metabolism (*6,7*) and viability (*8*). Several clinical trials using BMIPP have been undertaken to evaluate both ischemic heart disease (*9,10*) and hypertrophic cardiomyopathy (*10–12*). Despite these clinical trials, relatively little is known about the initial uptake and retention of BMIPP by the myocardium. The initial deposition of iodophenylpentadecanoic acid (IPPA), the parent iodinated fatty acid of BMIPP, has been shown to be proportional to regional myocardial blood flow (*13*). Therefore, we hypothesized that the initial uptake of BMIPP would also reflect myocardial blood flow. Accordingly, we compared the in vivo pattern of uptake of BMIPP and ^{201}Tl in normal and hypoperfused rabbit myocardium by quantitative dual-tracer autoradiography (Protocol I) and by segmental tissue analysis (Protocol II).

METHODS

Radiopharmaceutical

Iodine-125-BMIPP was suspended in an ursodesoxycholic acid phosphate salt solution. The manufacturer confirmed its radiochemical purity. BMIPP was used within the advised 2-mo period.

Protocol I

Surgical Procedure. New Zealand White male rabbits (n = 16) were anesthetized with 1%–2% isofluorane administered through an anesthesia apparatus. The carotid artery was catheterized and arterial pressure continuously recorded. The heart was exposed in a pericardial cradle through a left thoracotomy. A catheter was inserted into the left atrium to inject the radiolabeled microspheres. Rabbits were divided into occlusion (n = 13) and sham-operated control (n = 3) groups. The control group was used to evaluate the global uptake pattern of BMIPP in normal myocardium. Occlusion and sham-operated control groups for single-tracer ^{201}Tl were previously performed and reported by our group using a similar protocol (*14*) and were not repeated in this study. In the occlusion group, segmental hypoperfusion was produced by ligation of a major branch of the left circumflex artery. Radiolabeled microspheres (^{95}Nb, n = 5 × 10^5, diameter = 12–15 μm) were injected to document occlusion flow. Five minutes later, an intravenous injection of BMIPP (~150 μCi) was given and the tracer was allowed to circulate for 10 min. Five minutes into the circulation period, animals in the dual-tracer occlusion group were given an injection of ^{201}Tl (~750 μCi). The difference in circulation periods were to allow BMIPP time to potentially accumulate in ischemic tissue as previously described (*8,15*). After an addi-

Received Aug. 9, 1994; revision accepted Jan. 12, 1995.

For correspondence or reprints contact: Christopher P. Reinhardt, PhD, Department of Nuclear Medicine, University of Massachusetts Medical Center, 55 Lake Ave. N, Worcester, MA 01655-0243.

tional 5 min, the animals were killed. This intervention produced areas of normal flow and severe hypoperfusion separated by a sharply demarcated transition zone (*14*) without significant myocardial necrosis (*16,17*). Moreover, severe myocardial ischemia would result within the transition zone due to low myocardial blood flow (*18*). The longer circulation time for BMIPP compared to ^{201}Tl ensured accumulation of BMIPP within this transition zone before the animals were killed.

Autoradiography. The hearts were rinsed with saline and the atria excised. The ventricles were filled with embedding medium and then rapidly frozen in liquid nitrogen. Five consecutive ultrathin sections (30 μm) were collected on tape in a cryomicrotome at −20°C. The sections were air-dried at room temperature and mounted face-up on cardboard along with calibrated tissue paste standards of the same thickness (*19*). The sections and standards were placed directly on a sheet of single-coated x-ray film and then placed in a black plastic bag. The bag was vacuum-sealed, providing close apposition (2π geometry) between the film and sample. The sealed sample was set aside for exposure.

Quantitative autoradiography was performed for ^{201}Tl and BMIPP as previously described (*14*). Thallium-201 and ^{125}I were separated based on their different half-lives (73 hr versus 60.1 days for ^{201}Tl and ^{125}I, respectively) in the presence of an initial excess of ^{201}Tl. The first 15–18-hr exposure recorded the ^{201}Tl image. After ^{201}Tl had decayed (21 days), the samples were placed on a second sheet of film to record the ^{125}I image (25–50 days). This ^{125}I image also contained information about microsphere distribution as described below. Based on the quantitation of standard disks, ^{201}Tl-to-^{125}I and ^{125}I-to-^{201}Tl crossover was negligible. Only one exposure was required to image sections containing only [^{125}I]BMIPP (exposure time = 25–50 days). After the exposure period, the film was developed in an automatic x-ray film processor.

The difference in injected activity ensured that the dose (nCi · hr) delivered to the film emulsion was similar for the two radiopharmaceuticals. Film intensity measurements were converted to accumulated activity values, thereby enabling direct comparison.

Analysis of Autoradiographs. Representative autoradiographs from each experiment were digitized on a shielded lightbox with a video camera and dedicated image capture hardware. The images were signal-averaged to reduce noise, background-corrected to eliminate lightbox nonuniformity and recorded in a 512 × 512 matrix on a personal computer. Digitized images were analyzed using appropriate software.

Circumferential profile lines were drawn around the entire left ventricle at depths midway through both the subendocardium and subepicardium. For dual-tracer autoradiographs, image alignment was ensured by pinhole markers in conjunction with the image analysis software. The use of calibrated standards enabled the intensity value of each pixel along the profile to be converted to actual tracer activity concentration. Pixel intensity was converted to accumulated activity concentration, as previously described (*14*). Each accumulated activity curve was normalized to the mean accumulated activity concentration along the profile line. Defect contrast was calculated from the accumulated activity profiles as the ratio of normal-to-mean defect activities. Defect contrast for BMIPP was then compared to its corresponding ^{201}Tl value for each dual-tracer heart. Defect contrast values from dual-tracer hearts were compared to values obtained from single-tracer hearts. Relative defect size (as a percentage of the entire left ventricular wall) was determined by planimetry and compared for the tracers.

Determination of Relative Myocardial Blood Flow. Microspheres labeled with ^{95}Nb were chosen because of the low energy beta emission (β_{Max} = 159.8 keV: Yield = 5.5%) that produces discrete dark points on autoradiographs. Collectively, these discrete points form a "microsphere" image superimposed on the ^{125}I image. The microsphere content within the image was determined visually in the following manner: The left ventricular wall was subdivided into 16–32 segments divided equally between the subendocardial and subepicardial regions. These subdivisions were superimposed on the four additional contiguous images. The microsphere count in each segment in the subendocardial region was summated across the five images, then divided by the area of that segment. The microsphere concentration of each segment was then normalized to the mean regional microsphere concentration. These results were plotted with the normalized tracer activity curves, thus providing relative myocardial blood flow information across the subendocardium. This was repeated for the subepicardium. Pilot studies performed by our group suggest that the accuracy and reproducibility of this method of determining the relative microsphere tissue content is valid (*20*).

Protocol II

Surgical Procedure. Rabbits (n = 6) were anesthetized and surgically prepared as described above. Graded segmental hypoperfusion was produced with a micro-aneurysm clamp applied to a major branch of the left circumflex artery. Five minutes later, ^{95}Nb-labeled microspheres were injected through a left atrial catheter. Simultaneously, a 3-min reference blood sample was drawn from a femoral arterial catheter using an infusion pump. After completing the reference blood collection, BMIPP (~150 μCi) was injected intravenously and allowed to circulate for 10 min. Five minutes into the circulation period, ^{201}Tl (~200 μCi) was administered. Cardiac arrest was then induced by an intravenous injection of potassium chloride.

The hearts were quickly removed and rinsed with normal saline. The atria and right ventricle were excised. The left ventricle was frozen in preparation for segmental analysis.

Determination of Absolute Myocardial Blood Flow. Transmural left ventricle segments were weighed (55–76 segments/heart, 41 ± 21 mg/segment). Tracer activity was measured in a NaI (Tl) gamma well counter. All samples were corrected for inter-radionuclide crossover and tracer decay during the counting period. Tracer activity concentration was expressed as dpm/mg.

Absolute myocardial blood flow was determined as previously described (*21,22*). The myocardial microsphere content of each segment (dpm/mg) was normalized to the microsphere content measured in the 3-min reference blood collection (dpm · min/ml). The distributions of BMIPP and ^{201}Tl were correlated with absolute myocardial blood flow.

Arterial Blood Activity. Arterial blood-activity curves were generated for each rabbit. Thirty seconds after tracer injection, a 0.2-ml arterial blood sample was collected and placed into a preweighed test tube. Additional blood samples were collected at 1-min intervals for 10 min. Tracer activity was measured in a NaI (Tl) gamma well counter. All samples were corrected for inter-radionuclide crossover and tracer decay during the counting period. Tracer activity concentration was expressed as dpm/mg.

Statistics. Normal-to-defect contrast ratios and defect area from the dual-tracer hearts were compared using the Wilcoxon Matched-Pairs Signed-Ranks test. Contrast ratios and defect area from the single-tracer hearts were compared to dual-tracer hearts using the Mann-Whitney Rank Sum test of analysis of variance.

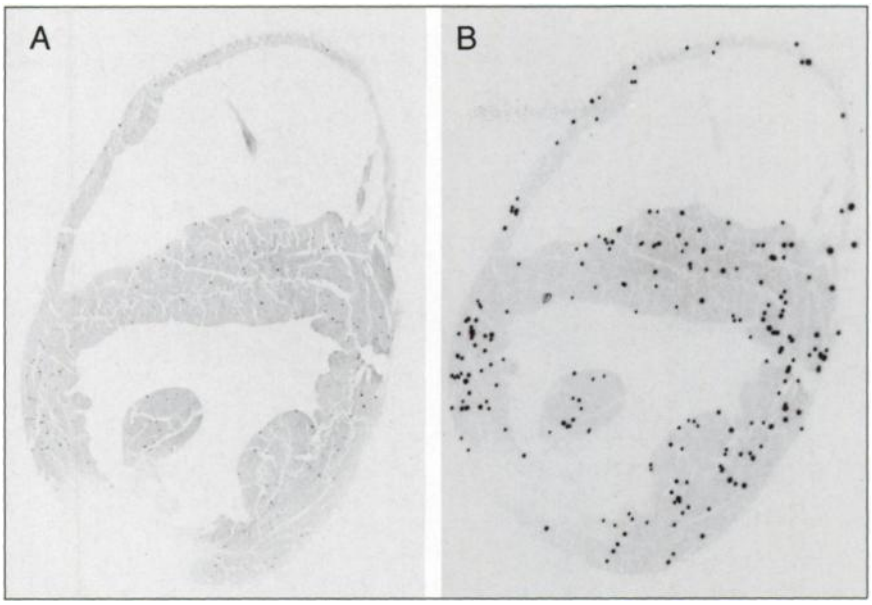

FIGURE 1. Representative autoradiographs. (A) Thallium-201 image which also contains a faint microsphere impression as a result of high-specific, local activity within each microsphere. (B) BMIPP and microsphere image.

RESULTS

Autoradiographic Analysis

For the dual-tracer hearts, the BMIPP autoradiographs subjectively appeared as sharply delineated as their corresponding ^{201}Tl autoradiographs (Fig. 1). Circumferential activity profiles for BMIPP paralleled those of ^{201}Tl in each dual-tracer heart (Fig. 2).

Normal-to-defect contrast ratio was defined as the accumulated activity concentration in the normal zone divided by the accumulated activity concentration in the low-flow zone (Table 1). The average contrast value for BMIPP was 23.1 ± 46.2 and 15.0 ± 25.5 for the subepicardium and subendocardium, respectively, while the average contrast value for ^{201}Tl was 18.4 ± 19.7 and 11.3 ± 14.5 for the subepicardium and subendocardium, respectively. No significant difference was observed between BMIPP and ^{201}Tl contrast values or between dual-tracer BMIPP and single-tracer BMIPP contrast values.

Relative defect size (as a percentage of the entire left ventricular wall) was determined by planimetry. For the dual-tracer autoradiographs, the average defect size was 21.3% ± 7.1% and 24.0% ± 11.1% for BMIPP and ^{201}Tl, respectively. The difference in BMIPP and ^{201}Tl defect size was not statistically significant nor was the difference between the defect size determined by dual- and single-tracer autoradiography.

Tracer Uptake Versus Relative Blood Flow (Protocol I)

Figure 3 displays the results when normalized tracer activity from segments in the subendocardial (n = 80) and subepicardial (n = 80) regions are plotted as a function of normalized microsphere concentration from dual-tracer autoradiographs. A strong, linear correlation results when BMIPP concentrations are plotted against ^{201}Tl concentrations.

A similar linear correlation was obtained from single-tracer autoradiographs that compared normalized BMIPP accumulated activity concentration to normalized microsphere concentration (Fig. 4).

Tracer Uptake Versus Absolute Blood Flow (Protocol II)

The myocardial activity concentrations of BMIPP and ^{201}Tl were compared to the absolute myocardial blood flow from transmural left ventricle segments (65 ± 7 segments/heart, 41 ± 21 mg/segment). An example of a strong, linear correlation between BMIPP and ^{201}Tl activity concentration as compared to myocardial blood flow is shown in Figure 5. Furthermore, in the same heart, a strong linear correlation was observed when the myocardial activity concentration of ^{201}Tl was plotted against BMIPP. The linear regression fits for all six hearts in Protocol II is shown in Table 2. These results are comparable to data (Fig. 3) obtained by segmental analysis of the autoradiographs (Protocol I). Specifically, the relative myocardial distribution of both ^{201}Tl and BMIPP are similar, utilizing quantitative autoradiography and segmental tissue analysis.

Blood Clearance (Protocol II)

Arterial blood activity curves were generated for each of the six rabbits. Initially, the activity concentration of BMIPP showed rapid blood clearance with a mean half-time ($t_{1/2,1}$) of 1.634 ± 0.404 min. Approximately 4 min after intravenous injection, however, ^{125}I blood activity increased, with a mean half-time ($t_{1/2,2}$) of 3.155 ± 0.403 min. The coefficients from the biexponential fit for each rabbit are shown in Table 3.

To obtain a blood activity curve past 10 min, one rabbit underwent Protocol II but was given only a single intravenous injection of BMIPP. After the initial 11 blood samples, an additional 14 samples were collected over a 2-hr period. The first 10-min period showed a similar rise in

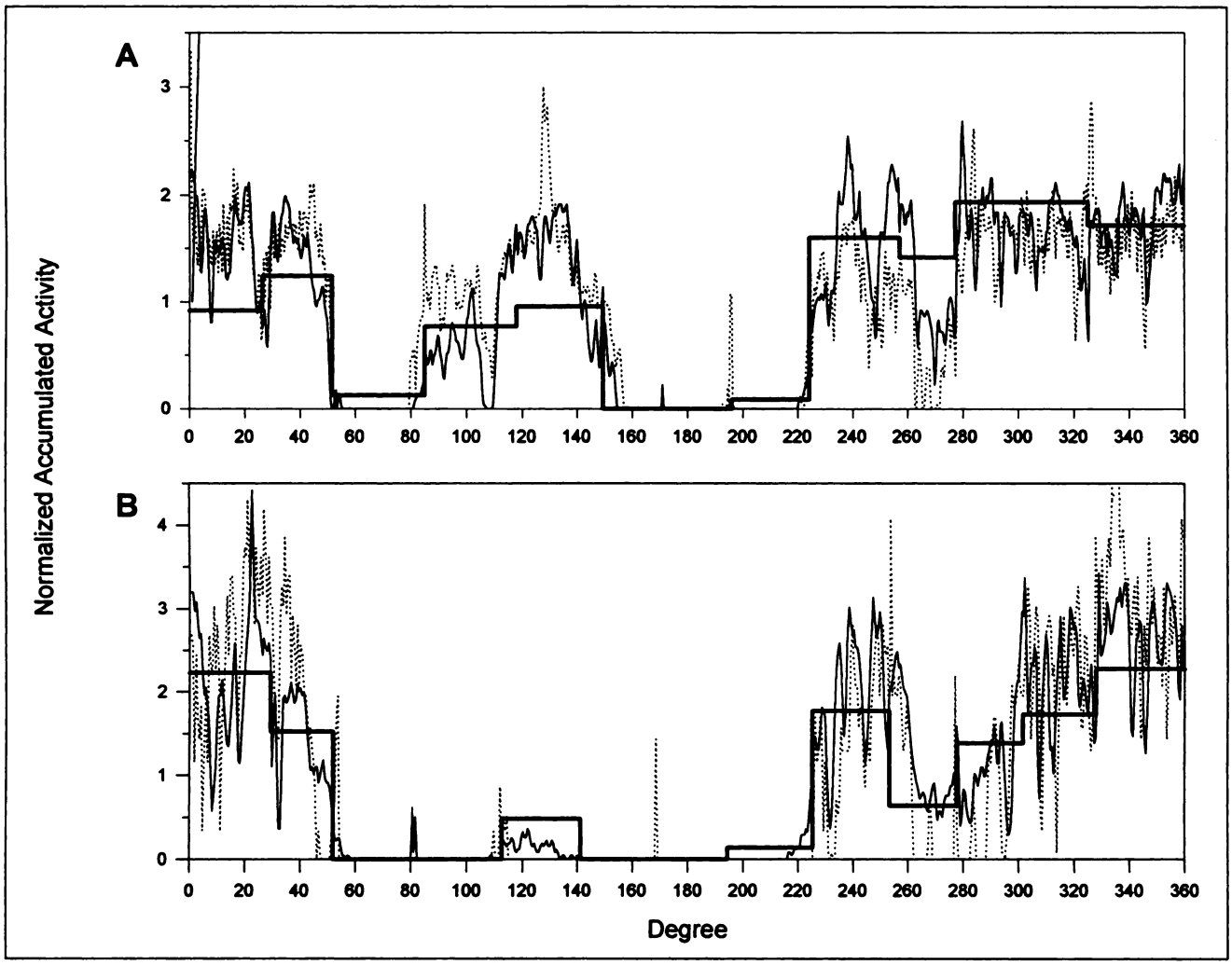

FIGURE 2. Circumferential activity profiles for [^{125}I]BMIPP (dotted lines) paralleled those of ^{201}Tl (thin solid lines) in both the subedicardium (plot A) and subendocardium (plot B). Both tracers conform to the regional blood flow determined by visual microsphere counting (thick solid lines).

arterial blood activity that began to plateau after 20 min (Fig. 6).

DISCUSSION

In this study, the initial deposition of BMIPP was shown to reflect coronary blood flow distal to an acute coronary occlusion. Dual-tracer autoradiographic activity profiles for BMIPP were comparable to those of ^{201}Tl. Moreover, the two tracers yielded similar results, both in normal-to-defect contrast and in defect size. Autoradiographic results (Protocol I) were comparable to those obtained from discrete tissue segments analyzed by gamma well counting (Protocol II). The myocardial activity concentration of BMIPP for both protocols correlated strongly with coronary blood flow at the time of tracer injection and compared favorably with ^{201}Tl, a standard tracer for myocardial perfusion scintigraphy. Therefore, differences in the myocardial distribution of BMIPP and ^{201}Tl in clinical studies may be related to cellular fatty acid metabolism (*9–12*) as opposed to differences in regional blood flow.

Quality Control

The conversion and Auger electrons associated with the decay of ^{125}I and ^{201}Tl are comparable. Therefore, the findings of this study cannot be attributed to differences in the linear energy transfer within the film emulsion. Single-tracer BMIPP autoradiographs produced similar results to dual-tracer BMIPP autoradiographs. Therefore, an error resulting from dual-tracer image contamination or from the effect of one tracer on uptake and retention of the other tracer is unlikely.

BMIPP Blood Kinetics

Nishimura et al. (*15*) studied a reperfused-postischemic canine model and found rapid blood clearance of [^{123}I]BMIPP. The mean half-time was reported as 0.83 ± 0.13 min. Ten minutes after intravenous injection, however, blood activity rose slightly. They attributed the rise in blood activity to the formation of metabolites in the liver. In six normal human volunteers, Torizuka et al. (*23*) observed a large rise in blood activity approximately 20 min

TABLE 1
Normal-to-Defect Contrast Ratios and Defect Size for Both Dual- and Single-Tracer Autoradiographs

Autoradiograph	Contrast				Defect size (%)	
	Subepicardium		Subendocardium			
Dual-Tracer	^{201}Tl	BMIPP	^{201}Tl	BMIPP	^{201}Tl	BMIPP
1	5.2	1.3	6.0	6.7	38.1	27.2
2	48.2	117.0	6.0	2.0	35.5	31.7
3	11.2	3.9	2.8	3.3	18.4	16.6
4	6.3	1.4	11.1	7.6	26.2	20.8
5	1.5	1.7	1.5	2.5	11.4	11.9
6	38.1	13.6	40.1	66.7	14.4	19.7
Mean ± s.d.	18.4 ± 19.7	23.1 ± 46.2	11.3 ± 14.5	15.0 ± 25.5	24.0 ± 11.1	21.3 ± 7.1
Single-Tracer		BMIPP		BMIPP		BMIPP
1		15.4		6.4		23.3
2		1.8		2.2		22.7
3		4.7		6.9		21.7
4		1.5		1.9		13.6
Mean ± s.d.		5.8 ± 6.5		4.4 ± 2.7		20.3 ± 4.6

after tracer injection. The rise in ^{123}I blood activity was later attributed to the metabolism of [^{123}I]BMIPP to [^{123}I]PIPA by alpha- and beta-oxidation processes within tissue (*24*).

Our findings show a similar rise in arterial blood activity in rabbits after 4 min that plateaus after 20 min to a relatively high level. This sharp rise in blood activity will contribute to background activity and may affect serial gamma camera assessment of BMIPP myocardial time-activity curves.

Advantages of the Method

Autoradiography provides high-resolution images from ultra-thin tissue sections. Film intensity is exponentially related to tracer activity (*25–27*) and this relationship varies with each film (*28*) and development process (*29,30*). Therefore, use of intensity or optical density values on autoradiographs is limited to cursory nonquantitative evaluation of tracer content. Our method permits a direct comparison between tracer activity profiles from two different radiolabeled tracers and microsphere determined myocardial blood flow. These quantitative autoradiographic observations were also confirmed by results obtained by gamma well counting, which is the gold standard for calculations of myocardial blood flow. Combining high-resolution autoradiographic analysis (Protocol I) and high-count rates associated with segmental analysis (Protocol II) allows for efficient evaluation of tracer deposition.

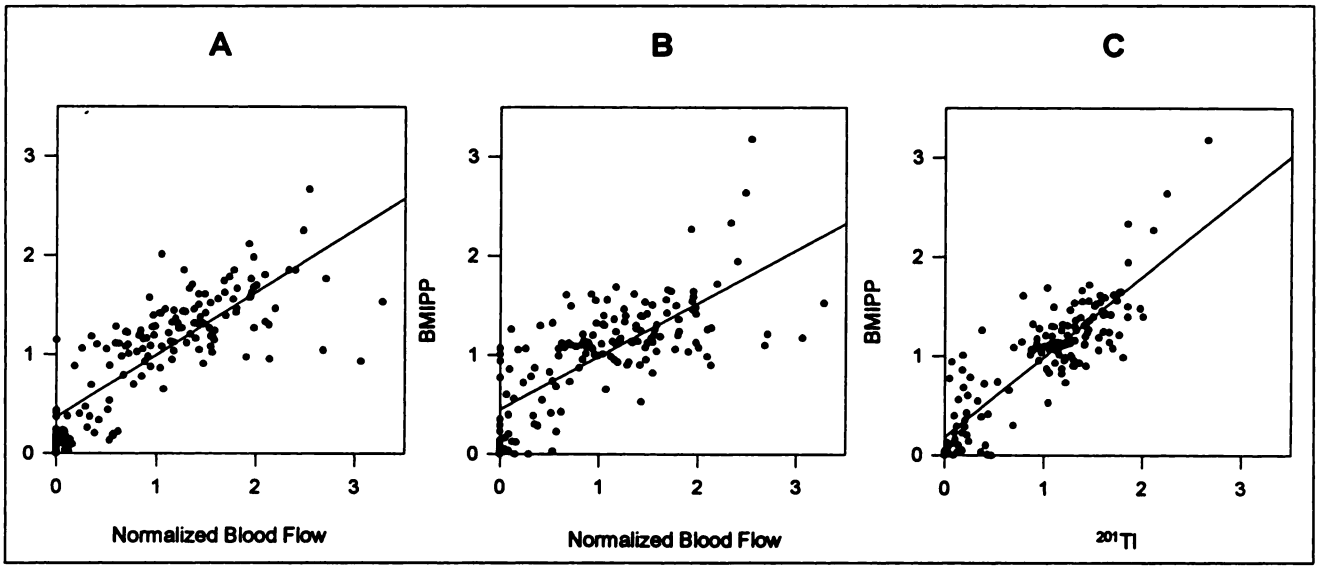

FIGURE 3. Based on dual-tracer autoradiographic analysis, microsphere determined normalized relative blood flow in both the subepicardium (n = 80) and subendocardium (n = 80) regions are plotted against its corresponding normalized ^{201}Tl concentration (plot A: y = 0.364 + 0.632x; r = 0.81) and normalized BMIPP concentration (plot B: y = 0.449 + 0.537x; r = 0.73). A strong linear correlation is noted when normalized BMIPP concentrations are plotted against normalized ^{201}Tl concentration (plot C: y = 0.181 + 0.806x; r = 0.86).

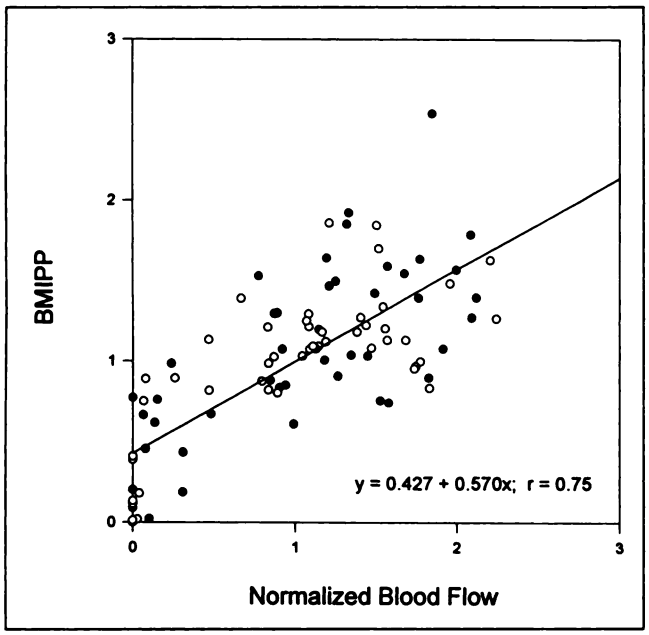

FIGURE 4. Based on single-tracer autoradiographic analysis, microsphere determined normalized relative blood flow in both the subepicardium (n = 48, hollow dots) and subendocardium (n = 48, solid dots) regions is plotted against its corresponding normalized BMIPP concentration.

BMIPP as a Marker of Myocardial Metabolism

Clinical experience suggests that a disparity of myocardial uptake between ^{201}Tl and BMIPP may have clinical relevance. Typically, this involves segments with less BMIPP uptake than ^{201}Tl (*9–12*). Some experimental studies have been published that are important to review in this potential context (*8,15,31*).

In a reperfused, postischemic canine model, the uptake of BMIPP was evaluated for its effectiveness as a noninvasive marker of altered fatty acid metabolism (*15*). After 3 hr of occlusion followed by 3 hr of reperfusion, [^{123}I]BMIPP was administered and serial myocardium images were collected every 3 min. After 15 min, ^{201}Tl was administered and static images of both [^{123}I]BMIPP and ^{201}Tl were collected. The hearts were later excised and sectioned for ex vivo imaging on an Anger camera. No corrections were made for radionuclide crossover. Image analysis showed increased uptake of BMIPP in the reperfused area as compared to ^{201}Tl. A recent report (*32*), evaluating clinical techniques of dual-radionuclide imaging, clearly demonstrates that uncorrected images can be misinterpreted due to Compton scatter and radionuclide crossover artifacts. Thallium-201 has a 10% probability of emitting a 167-keV photon. As a result, the imaging window set for BMIPP (^{123}I, y = 159 keV) will also record the ^{201}Tl photon. Therefore, differences observed on uncorrected images should be interpreted with caution. If this experimental model is correct, then ^{201}Tl uptake would be less comparable to BMIPP, which is in opposition to the observed clinical studies.

Miller et al. (*8*) used a reperfused canine model to relate the myocardial distribution of BMIPP to myocardial blood flow. Their results showed disproportionally high retention of BMIPP compared to microsphere determined blood flow in reperfused, severely ischemic myocardium but reduced BMIPP activity in infarcted segments. Their conclusions are largely based on segmental activity concentrations determined after incubation in the vital tissue stain triphenyl tetrazolium chloride (TTC) for approximately 3 hr. No reference was made to the possible effect this vital stain might have on BMIPP. In a recent publication (*33*), our group reported that the postmortem distribution of radio-

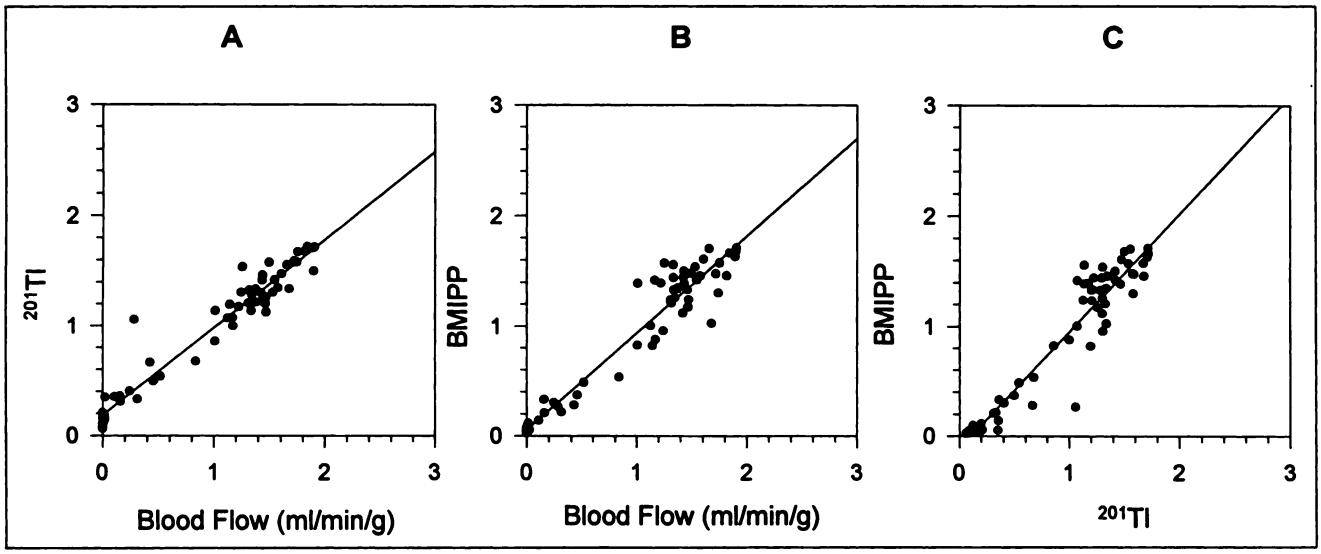

FIGURE 5. Based on dual-tracer segmental tissue analysis, microsphere determined normalized absolute blood flow (ml/min/g) is plotted against its corresponding normalized ^{201}Tl concentration (plot A: y = 0.187 + 0.796x; r = 0.95) and normalized BMIPP concentration (plot B: y = 0.058 + 0.881x; r = 0.94). A strong linear correlation results when normalized BMIPP concentrations are plotted against normalized ^{201}Tl concentrations (plot C: y = −0.111 + 1.065x; r = 0.92).

TABLE 2
Linear Regression Fits Obtained from Six Rabbit Hearts

No.	^{201}Tl vs. Blood flow	BMIPP vs. Blood flow	BMIPP vs. ^{201}Tl
1	y = 0.187 + 0.796x; r = 0.95	y = 0.058 + 0.881x; r = 0.94	y = −0.111 + 1.065x; r = 0.92
2	y = 0.484 + 0.725x; r = 0.75	y = 0.447 + 0.760x; r = 0.73	y = −0.063 + 1.051x; r = 0.97
3	y = 0.201 + 0.975x; r = 0.96	y = 0.298 + 0.814x; r = 0.92	y = 0.163 + 0.802x; r = 0.92
4	y = 0.226 + 0.870x; r = 0.94	y = 0.234 + 0.825x; r = 0.91	y = 0.038 + 0.929x; r = 0.94
5	y = 0.175 + 1.116x; r = 0.99	y = 0.192 + 1.091x; r = 0.97	y = 0.022 + 0.976x; r = 0.98
6	y = 0.321 + 0.984x; r = 0.85	y = 0.350 + 0.928x; r = 0.75	y = 0.086 + 0.905x; r = 0.87

The first experiment is depicted in Figure 4.

pharmaceuticals can be affected by exposure to TTC. Furthermore, TTC has been shown to accelerate washout of certain tracers from damaged myocardial cells (*34*). Therefore, TTC should not be assumed as inert. If exposure to TTC chemically effects either the structure of BMIPP or the tissue binding sites for BMIPP, then the determination of tissue tracer concentration must be made prior to histochemical staining.

TABLE 3
Half-Times Obtained from Bi-exponential Fitting of Arterial Blood Collections for Six Rabbits

No.	BMIPP blood clearance $T_{1/2,1}$ (min)	BMIPP blood clearance $T_{1/2,2}$ (min)
1	1.070	3.108
2	2.133	2.484
3	1.462	3.648
4	1.631	3.431
5	1.447	3.270
6	2.063	2.988
Average	1.634 ± 0.404	3.155 ± 0.403

Arterial blood activity = $a \cdot e^{-(\ln 2/t_{1/2,1})T}$ (initial drop) + $b \cdot e^{+(\ln 2/t_{1/2,2})T}$ (initial rise).

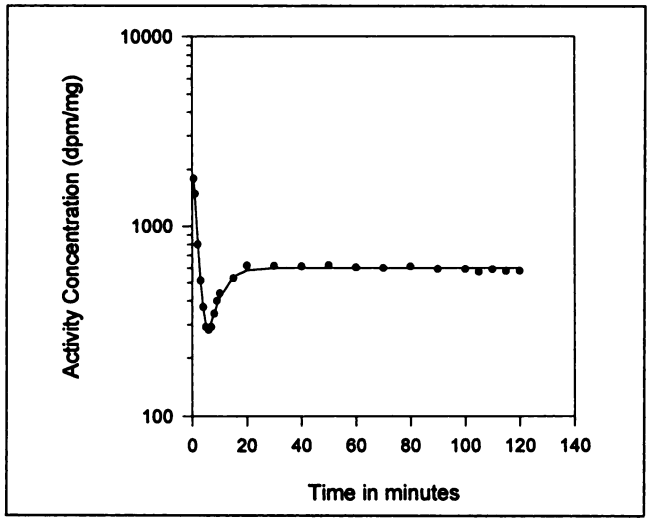

FIGURE 6. Arterial blood-activity curve for BMIPP. Data were obtained from one rabbit over a 2-hr circulation period.

Kurata et al. (*31*) used a cardiomyopathic model to investigate the distribution of ^{201}Tl and [^{125}I]BMIPP by dual-tracer autoradiography. Tracer uptake was determined directly from optical density ratios. The film density ratio for BMIPP was significantly lower than ^{201}Tl in cardiomyopathic hamsters but not in normal, control hamsters. By comparison, Syrian hamsters that were pretreated with verapamil to retard disease progression showed no significant difference in regional concentration of BMIPP and ^{201}Tl. Because of the logarithmic response of the film (*25–27*), however, an optical density ratio is really only a qualitative assessment that may lead to an artifactual interpretation of tracer distribution and contrast patterns. Given these experimental limitations, the observations of Miller et al. (*8*) and Kurata et al. (*31*) could be used to support current clinical results.

As noted above, these in vivo observations (*8,15,31*) should be interpreted cautiously in view of possible methodological problems. In this study, however, care was taken to avoid similar problems. Our study clearly demonstrates that the initial deposition of BMIPP, like ^{201}Tl, will reflect coronary blood flow in the presence of an acute coronary occlusion. Therefore, differences observed between the retention of BMIPP and ^{201}Tl may be related to myocardial fatty acid metabolism. Presently, the uptake characteristics of BMIPP are based on a limited number of in vivo animal studies. Additional studies that examine BMIPP clearance in metabolically altered myocardium are still warranted.

APPENDIX

Radioisotope analysis by autoradiography produces high-resolution images of isolated ultrathin myocardial slices. Film intensity is exponentially related to tracer activity, and this relationship varies with each film and development process. Therefore, the use of intensity per se on autoradiographs is limited to the cursory nonquantitative evaluation of tracer content. The method described here, however, can generate accumulated activity concentration values and allows tracer activity to be determined at any point in the myocardial slice. Two or more isotopes that differ in half-life can be studied simultaneously with judiciously chosen injected doses.

Conversion of Intensity to Activity

For each experiment, samples of tissue paste standards were weighed and counted in a NaI (Tl) gamma counter and corrected for decay. The activity concentration of each sample (dpm/mg) was determined based on the counting efficiency of the detector for ^{201}Tl and ^{125}I. For each set of standard discs, the accumulated activity contained in each standard disc was graphed against its average intensity on a semi-log plot. The accumulated activity, $\tilde{A}$, contained in a given standard disc during the film exposure was calculated as follows:

$$\tilde{A} = Ame^{\lambda t_1} \int_0^{t_2} e^{-\lambda t}\, dt,$$

where A = the activity of the standard measured in the gamma counter (dpm/mg); m = the mass of a 30μ standard disc (0.85 mg); λ = the decay constant of the radioisotope (s^{-1}); t_1 = the interval between the start of the exposure and the counting of the standards in the gamma counter(s); and t_2 = the duration of the exposure(s). The response of photographic film to radiation exposure is nonlinear, as defined by the H & D curve. Therefore, the results of each set of standards were then fit, using the least squares method, to a sigmoidal function defined as follows:

$$I = \frac{(a - d)}{1 + \left(\frac{\tilde{A}}{c}\right)^b} + d,$$

where I = the corresponding intensity value; a = a constant which represents the maximum intensity value; b = a constant that describes the steepness of the curve; c = a constant that represents the accumulated activity value at the inflection point; and d = a constant that represents the minimum intensity value. Intensity data were thereby converted to accumulated activity using the parameters obtained from the above fit. The actual myocardial accumulated activity values spanned the region from ~10–1000 nCi-hr.

ACKNOWLEDGMENTS

The authors thank Drs. Seth Dahlberg and Bernard Villegas for their useful discussions and Harriet Kay for editorial assistance. They also thank Takashi Sakoda (Nihon Medi-Physics) for product support and encouragement. This manuscript was supported in part by National Institutes of Health research grant RO1 HL 34199.

REFERENCES

1. Hütter JF, Soboll S. Role of fatty acid metabolites in the development of myocardial ischemic damage. *Int J Biochem* 1992;24:399–403.
2. Lochner A, Kotzè JCN, Benade AJS, Gevers W. Mitochondrial oxidative phosphorylation in low-flow hypoxia: role of free fatty acids. *J Mol Cell Cardiol* 1978;10:857–875.
3. Schön HR, Schelbert HR, Najafi A, et al. Carbon-11-labeled palmitic acid for the noninvasive evaluation of regional myocardial fatty acid metabolism with positron-computed tomography: II. Kinetics of C-11 palmitic acid in acutely ischemic myocardium. *Am Heart J* 1982;103:548–561.
4. Schön HR, Schelbert HR, Robinson G, et al. Carbon-11-labeled palmitic acid for the noninvasive evaluation of regional myocardial fatty acid metabolism with positron-computed tomography: I. Kinetics of C-11 palmitic acid in normal myocardium. *Am Heart J* 1982;103:532–547.
5. Weiss ES, Hoffman EJ, Phelps ME, et al. External detection and visualization of myocardial ischemia with ^{11}C-substrates in vitro and in vivo. *Circ Res* 1976;39:24–32.
6. Ambrose KR, Owen BA, Goodman MM, Knapp FF Jr. Evaluation of the metabolism in rat hearts of two new radioiodinated 3-methyl-branched fatty acid myocardial imaging agents. *Eur J Nucl Med* 1987;12:486–491.
7. Knapp FF Jr., Goodman MM, Callahan AP, Kirsch G. Radioiodinated 15-(p-iodophenyl)-3, 3-dimethylpentadecanoic acid: a useful new agent to evaluate myocardial fatty acid uptake. *J Nucl Med* 1986;27:521–531.
8. Miller DD, Gill JB, Livni E, et al. Fatty acid analogue accumulation: a marker of myocyte viability in ischemic-reperfused myocardium. *Circ Res* 1988;63:681–692.
9. Tamaki N, Kawamoto M, Yonekura Y, et al. Regional metabolic abnormality in relation to perfusion and wall motion in patients with myocardial infarction: assessment with emission tomography using an iodinated branched fatty acid analog. *J Nucl Med* 1992;33:659–667.
10. Nishimura T, Uehara T, Shimonagata T, Nagata S, Haze K. Clinical results with β-methyl-p-(^{123}I)iodophenylpentadecanoic acid, single-photon emission computed tomography in cardiac disease. *J Nucl Cardiol* 1994;1:S65–S71.
11. Kurata C, Tawarahara K, Taguchi T, et al. Myocardial emission computed tomography with iodine-123-labeled beta-methyl-branched fatty acid in patients with hypertrophic cardiomyopathy. *J Nucl Med* 1992;33:6–13.
12. Takeishi Y, Chiba J, Abe S, et al. Heterogeneous myocardial distribution of iodine-123 15-(p-iodophenyl)-3-R,S-methylpentadecanoic acid (BMIPP) in patients with hypertrophic cardiomyopathy. *Eur J Nucl Med* 1992;19:775–782.
13. Caldwell JH, Martin GV, Link JM, Krohn KA, Bassingthwaighte JB. Iodophenylpentadecanoic acid-myocardial blood flow relationship during maximal exercise with coronary occlusion. *J Nucl Med* 1990;30:99–105.
14. Weinstein H, Reinhardt CP, Leppo JA. Teboroxime, sestamibi and thallium-201 as markers of myocardial hypoperfusion: comparison by quantitative dual-isotope autoradiography in rabbits. *J Nucl Med* 1993;34:1510–1517.
15. Nishimura T, Sago M, Kihara K, et al. Fatty acid myocardial imaging using ^{123}I-β-methyl-iodophenyl pentadecanoic acid (BMIPP): comparison of myocardial perfusion and fatty acid utilization in canine myocardial infarction (occlusion and reperfusion model). *Eur J Nucl Med* 1989;15:341–345.
16. Connelly CM, Vogel WM, Hernandez YM, Apstein CS. Movement of the necrotic wavefront after coronary occlusion in the rabbit. *Am J Physiol* 1982;243:H682–H690.
17. Miura T, Downey JM, Ooiwa H, Ogawa S, Adachi T, et al. Progression of myocardial infarction in a collateral flow-deficient species. *Jpn Heart J* 1989;30:695–708.
18. Harken AH, Simson MB, Haselgrove J, et al. Early ischemia after complete coronary ligation in the rabbit, dog, pig and monkey. *Am J Physiol* 1981; 241:H202–H210.
19. Ito T, Brill AB. Validity of tissue paste standards for quantitative whole-body autoradiography using short-lived radionuclides. *Appl Radiat Isot* 1990;41:661–667.
20. Reinhardt CP, Weinstein H, Marcel R, Leppo JA. Regional blood flow determination by autoradiographic microsphere imaging [Abstract]. *J Nucl Med* 1994;35:180P.
21. Heyman MA, Payne BD, Hoffman JIE, Rudolph AM. Blood flow measurement with radionuclide-labeled particles. *Prog Cardiovasc Dis* 1977;20:55–79.
22. Connelly CM, Leppo JA, Weitzman PW, Vogel WM, Apstein CS. Effect of coronary occlusion and reperfusion on myocardial blood flow during infarct healing. *Am J Physiol* 1989;257:H365–H374.
23. Torizuka K, Yonekura Y, Nishimura T, Tamaki N, Uehara T, et al. The phase 1 study of β-methyl-p-(^{123}I)-iodophenyl-pentadecanoic acid (^{123}I-BMIPP). *Jpn J Nucl Med* 1991;28:681–690.
24. Okano S, Yoshimura H, Okano K, et al. Metabolite of 15-p-iodophenyl-3(R,S)-pentadecanoic acid (^{123}I) in blood and urine. *Jpn J Nucl Med* 1992; 29:1489–1493.
25. Swillens S, Cochaux P, Lecocq R. A pitfall in the computer-aided quantitation of autoradiograms. *Trends Biochem Sci* 1989;14:440–441.
26. Wagner LK, Barnes GT, Bencomo JA, Haus AG. An examination of errors in characteristic curve measurements of radiographic screen/film system. *Med Phys* 1983;10:365–369.
27. Johns HE, Cunninghan JR. Diagnostic radiology. In: *The physics of radiology*, 4th ed. Springfield, IL: Charles C. Thomas, 1983:557–669.
28. Jackson VP, Harrill CD, White SJ, Gillespie KR, Mail JT, et al. Evaluation of a dual-screen, dual-emulsion mammography system. *Am J Roentgenol* 1989;152:483–486.
29. Faix CD, Van Tuinen R, Kereiakes JG. Quality control for automated film processing. *Radiol Technol* 1973;44:257–782.
30. Kimme-Smith C, Rothschild PA, Bassett LW, Gold RH, Moler C. Mam-

mographic film-processor temperature, development time, and chemistry: effect on dose, contrast and noise. *Am J Roentgenol* 1989;152:35–40.
31. Kurata C, Kobayashi A, Yamazaki N. Dual-tracer autoradiographic study with thallium-201 and radioiodinated fatty acid in cardiomyopathic hamsters. *J Nucl Med* 1989;30:80–87.
32. Weinstein H, King MA, Reinhardt CP, McSherry B, Leppo JA. A method of simultaneous dual radionuclide cardiac imaging with ^{99m}Tc and ^{201}Tl. Part I: analysis of inter-radionuclide crossover and validation in phantoms. *J Nucl Cardiol* 1994;1:39–51.
33. Reinhardt CP, Weinstein H, Wironen J, Leppo JA. Effect of triphenyl tetrazolium chloride staining on the distribution of radiolabeled pharmaceuticals. *J Nucl Med* 1993;34:1722–1727.
34. Villegas BJ, Reinhardt CP, Dahlberg ST, Heller LI, Leppo JA. Sestamibi distribution in viable and nonviable myocardium assessed independent of the vital stains [Abstract]. *J Nucl Med* 1994;35(suppl):152P.

(continued from page 1538)

FIRST IMPRESSIONS:
METASTATIC CALCIFICATIONS IN HYPERPARATHYROIDISM

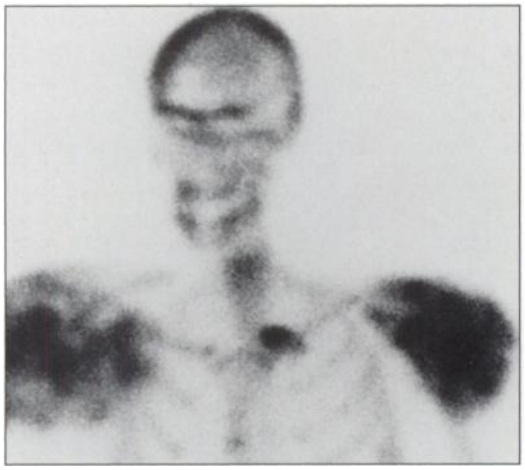

FIGURE 1.

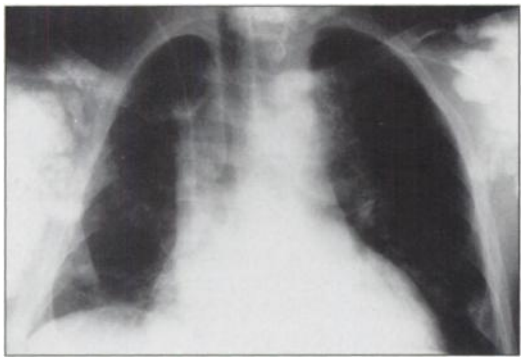

FIGURE 2.

PURPOSE
A 26-yr-old man with end-stage renal disease and secondary hyperparathyroidism was referred for a ^{99m}Tc-pyrophosphate study to evaluate his recently transplanted kidney for acute tubular nephrocalcinosis. On physical exam, the patient was noted to have huge shoulders out of proportion to his thin stature, with a palpable doughy consistency. The ^{99m}Tc-pyrophosphate scan revealed extensive globular, markedly increased tracer uptake overlying both shoulders with a focus of activity in the head of the left clavicle corresponding to a brown tumor seen on radiography (Fig. 1). Chest radiography revealed massive flocculent soft-tissue calcification in both the axillary and shoulder regions, consistent with secondary hyperparathyroidsim (Fig. 2). Surgery demonstrated marked parathyroid gland hyperplasia.

TRACER
Technetium-99m-pyrophosphate, 22 mCi (814 MBq)

ROUTE OF ADMINISTRATION
Intravenous

TIME AFTER INJECTION
2 hours

INSTRUMENTATION
Hitachi Spectrum LFOV gamma camera with LEAP collimation

CONTRIBUTORS
Charles W. Sutter, David K. Shelton, University of California, Davis Cancer Center, Sacramento, CA